Investigating the Talbot Effect in Arrays of Optical Dipole Traps for Neutral Atom Quantum Computing

A Senior Project
presented to
the Faculty of the Physics Department
California Polytechnic University, San Luis Obispo

In Partial Fulfillment
of the Requirements for the Degree
Bachelor of Science

By

Sergio Aguayo

April 2, 2019

Abstract

Quantum computers are devices that are able to perform calculations not achievable for classical computers. Although there are many methods for creating a quantum computer, using neutral atoms offers the advantage of being stable when compared to other methods. The purpose of this investigation is to explore possible optical dipole trap configurations that would be useful for implementing a quantum computer with neutral atoms. Specifically, we computationally investigate arrays of pinholes, the diffraction pattern generated by them, and the onset of the Talbot effect in these traps. We manipulate the radius of the pinholes, the number of pinholes in the array, and the distance between adjacent pinholes in order to create trap configurations where the presence/absence of the Talbot effect contributes to the usefulness of the trap for quantum computing. We find configurations with pinhole distances of 80 μm and 100/110 μm respectively satisfied an absence and a strong presence of the Talbot effect.

Contents

List of Figures

1 Introduction

Quantum computers are devices which can perform tasks unreachable for classical computers. The property separating quantum computers and classical computers are their units of data: qubits and bits. Bits are units with two possible values–0 or 1; on the other hand, qubits take advantage of superposition to create states characterized as linear combinations of 0 and 1. Just like with classical computers, quantum computers have logic gates that can be used to perform calculations or solve computational problems. Logic gates can involve any number of qubits, requiring that qubits be entangled and that individual qubit's states be manipulated. This necessitates precise control of qubits, meaning that there are certain criteria that must be met by the hardware infrastructure of a quantum computer.

There are five requirements needed for implementing a quantum computer: (1) A scalable physical system with well characterized qubits; (2) the ability to initialize the state of qubits to a simple state; (3) long decoherence times that are much longer than gate operation times; (4) a universal set of quantum gates; (5) the ability to measure qubit states [1].

While there are several different ways to implement a quantum computer, the one we focus on uses neutral atoms. Neutral atoms have the advantage of being relatively stable compared to the components of other implementations. This leads to an advantage in (3)–long decoherence times–and in (1)–the ability to scale the system. Since neutral atoms are so stable, not only do we get long decoherence times, we are also able to scale a system to a large number in a small amount of space, since nearby atoms rarely interact with one another [2].

The aim of this project is to model possible traps that will fulfill the listed criteria for implementing a quantum computer. This will be accomplished using atomic dipole traps. Atomic dipole traps utilize electric dipole interaction with light [3]. These traps are created by passing a laser beam through a pinhole, which produces a diffraction pattern. The intensity gradient of these diffraction patterns interact with the induced dipole moment in a neutral atom to create a potential well. The minima of the potential well can be used as an atom trap [3].

Typically, trapping is limited to one trap per diffraction pattern, meaning we trap one atom per pinhole. Since we want to create traps useful for quantum computing, we need to use more than one pinhole. This is easily done by creating a mask with an arrangement of pinholes (such as a 1D or 2D array of pinholes). However, introducing these periodic arrangement of pinholes results in a periodic reproduction of the pinhole arrangement in the diffraction pattern. This periodic reproduction is known as the Talbot effect. Depending on the desired result, the Talbot effect can be a disadvantage or an advantage to your trap. This project explores how the Talbot effect can be avoided or used in order to produce a trap configuration useful for quantum computing.

2 Theory

2.1 Realization of Qubits

The five criteria listed in Section 1 create restrictions for what our atom traps can look like. These restrictions and our ideal trap configurations will be discussed in this section.

Criterion (1) requires that our system be scalable. To do this, the trap created should have well defined locations. An example of what traps may look like are two-dimensional rectangular arrays or three-dimensional rectangular arrays.

Criteria (2), (4), and (5) require that we have the ability to initialize qubits and have the ability to measure their states. This means that it is advantageous that each atom be individually addressable. Atoms can be individually addressed using lasers. In a two-dimensional array, addressing individual atoms can be done by shining a laser on an atom perpendicular to the plane of the array. Descriptions of two-dimensional arrays can be seen in [4] and [5]. Addressing individual atoms in a three-dimensional array is more of a challenge, but it is achievable. Addressing individual atoms in a three-dimensional array has been achieved using pulsed microwaves and two laser beams [2].

With these criteria in mind, we can plan what atom traps can look like. Two-dimensional and three-dimensional arrays are both viable options and have been shown to be able to meet the listed criteria.

2.2 Neutral Atom Traps

The type of neutral atom trap we are using is an optical dipole trap. As discussed in Section 1, optical dipole traps utilize the interaction between the intensity gradient of light and the induced electric dipole of a neutral atom. In this section, we will detail this interaction.

Light used in an optical dipole trap is far-detuned from the resonance frequency of a transition in the atom. This allows us to neglect forcing from radiative pressures (the pressure created by recoils due to photon absorption) [3] and to treat the light classically as a harmonic driving field with angular frequency ω. This electric field $\mathbf{E}$ induces an electric dipole $\mathbf{p}$ in the atom.

The electric field is written in complex notation: $\mathbf{E}(\mathbf{r}, t) = E_o e^{-i\omega t}$. Dipole moments are defined as $\mathbf{p} = q\mathbf{d}$, where q is the charge at either end of the dipole, and $\mathbf{d}$ is the displacement vector from the negative charge to the positive charge. If we take the nucleus of the atom as the center of our system and $\mathbf{x}$ as the position vector of the electron orbiting the nucleus, then we have $\mathbf{d} = -\mathbf{x}$, which gives $\mathbf{p} = -e\mathbf{x}$, where e is the elementary charge.

We can solve for the position vector of the electron by treating the motion of the electron as a driven and damped oscillation around the nucleus. This gives us a differential equation

$$m_e \frac{d^2x}{dt^2} + m_e \Gamma_\omega \frac{dx}{dt} + m_e \omega_o^2 x = -eE_o e^{-i\omega t}, \tag{1}$$

where m_e is the mass of an electron, Γ_ω is the radiative decay rate of the energy of an electron oscillating at an angular frequency ω in an atom, and ω_o is the resonance angular frequency of the atom [6]. Solving this equation gives

$$x = -\frac{e}{m_e}\frac{1}{\omega_o^2 - \omega^2 - i\omega\Gamma_\omega}E_o e^{-i\omega t}. \tag{2}$$

Which gives

$$\mathbf{p} = \frac{e^2}{m_e}\frac{1}{\omega_o^2 - \omega^2 - i\omega\Gamma_\omega}E_o e^{-i\omega t}\hat{\mathbf{x}}. \tag{3}$$

We can simplify the expression for $\mathbf{p}$ by introducing variable α, defined as

$$\alpha = \frac{e^2}{m_e}\frac{1}{\omega_o^2 - \omega^2 - i\omega\Gamma_\omega}, \tag{4}$$

which simplifies $\mathbf{p}$ to

$$\mathbf{p} = \alpha\mathbf{E}. \tag{5}$$

Now that we have established the relationship between the dipole moment and the electric field, we can move on to describing the potential energy of our trap. The potential energy of a dipole moment in an electric field is given by

$$U_{dip} = -\mathbf{p}\cdot\mathbf{E}. \tag{6}$$

However, since our electric field and dipole oscillate so rapidly, only their time averages are relevant [6]. Also, since our atom is an induced dipole moment, we need to introduce a factor of 1/2 [6]. This gives

$$U_{dip} = -\frac{1}{2}\langle\mathbf{p}\cdot\mathbf{E}\rangle. \tag{7}$$

Since our dipole moment and electric field are in complex notation, we need to find their real parts in order to use them in the U_{dip} equation. The real part of the electric field is given by

$$\mathrm{Re}(\mathbf{E}) = E_o\cos(\omega t)\hat{\mathbf{x}}, \tag{8}$$

and the real part of the dipole moment is given by

$$\begin{aligned}\mathrm{Re}(\mathbf{p}) &= \mathrm{Re}(\alpha)\,\mathrm{Re}(\mathbf{E}) + \mathrm{Im}(\alpha)\,\mathrm{Im}(\mathbf{E}) \\ &= E_o\left(\mathrm{Re}(\alpha)\cos(\omega t) - \mathrm{Im}(\alpha)\sin(\omega t)\right)\hat{\mathbf{x}}.\end{aligned} \tag{9}$$

Plugging $\mathrm{Re}(\mathbf{p})$ and $\mathrm{Re}(\mathbf{E})$ into equation 7, we obtain

$$U_{dip} = -\frac{1}{4}\frac{e^2}{m_e}\frac{\omega_o^2 - \omega^2}{(\omega_o^2 - \omega^2)^2 + \omega^2\Gamma_\omega^2}E_o^2. \tag{10}$$

This expression can be simplified by introducing the linewidth of the atom at resonance Γ and the saturation field E_s. We start with Γ_ω, the radiative decay rate of the energy of an electron oscillating at an angular frequency ω defined as $\Gamma_\omega = \frac{e^2\omega^2}{6\pi\epsilon_o m_e c^3}$. For an atom at resonance (ie. $\omega = \omega_o$), we have $\Gamma = \frac{e^2\omega_o^2}{6\pi\epsilon_o m_e c^3}$. Putting these together, we get an expression for Γ_ω in terms of Γ:

$$\Gamma_\omega = \frac{\omega^2}{\omega_o^2}\Gamma. \tag{11}$$

Now we consider the saturation field E_s. The expression for the saturation field is [6]

$$E_s^2 = \frac{\hbar\Gamma^2 m_e \omega_o}{e^2}, \tag{12}$$

where $\hbar$ is Planck's constant. Substituting the expressions for the saturation field and the linewidth of the atom at resonance into U_{dip} yields

$$U_{dip} = -\frac{\hbar\Gamma^2\omega_o}{4}\frac{\omega_o^2 - \omega^2}{\left(\omega_o^2 - \omega^2\right)^2 + \left(\frac{\omega^3}{\omega_o^2}\right)^2\Gamma^2}\frac{E^2}{E_s^2}. \tag{13}$$

Further simplification of this expression can be achieved by considering two approximations: the first is $\left(\omega_o^2 - \omega^2\right)^2 >> \left(\frac{\omega^3}{\omega_o^2}\right)^2\Gamma^2$, and the second is that ω_o and ω are the same order of magnitude. With these approximations we simplify U_{dip} to

$$U_{dip} = \frac{\hbar\Gamma}{8}\frac{\Gamma}{\Delta}\frac{E_o^2}{E^2}, \tag{14}$$

where Δ is the amount of laser detuning $\omega - \omega_o$.

2.3 Pinhole Diffraction

In order to properly model our trap, we need to calculate the electric field of the diffraction pattern. This is done by using Fresnel scalar diffraction theory. Our start point for our calculation is to consider the Fresnel-Kirchhoff diffraction integral. This equation gives the electric field $\mathbf{E}$ of the diffracted light at point P_1 and is defined as

$$\mathbf{E}(P_1) = \frac{kz_1}{i2\pi}\iint_{S_o}\mathbf{E}_{z=0}\frac{e^{ik\rho}}{\rho^2}\,dx_o\,dy_o, \tag{15}$$

where k is the wavenumber of the light used, S_o is the surface of the pinhole, $\mathbf{E}_{z=0}$ is the electric field on the plane of the pinhole, and

$$\rho = \sqrt{(x_1 - x_0)^2 + (y_1 - y_0)^2 + z_1^2}, \tag{16}$$

where the variables with subscript 0 are in the plane of the pinhole and the variables with subscript 1 are at the point of interest P_1.

If we use binomial expansion on ρ it becomes

$$\rho = \sum_{n=0}^{\infty} \binom{1/2}{n} \frac{((x_1 - x_0)^2 + (y_1 - y_0)^2)^n}{z_1^{2n-1}}. \tag{17}$$

By taking approximations $z_1^3 >> \frac{\pi}{4\lambda}((x_1 - x_0)^2 + (y_1 - y_0)^2)^2$ and $\rho^2 \approx z_1^2$ we can reduce $k\rho$ into

$$k\rho = \frac{2\pi}{\lambda}\left(z_1 + \frac{1}{2}\frac{(x_1 - x_0)^2 + (y_1 - y_0)^2}{z_1}\right) \tag{18}$$

and the Fresnel-Kirchhoff diffraction integral into

$$E(P_1) = \frac{ke^{ikz_1}}{i2\pi z_1} \iint E_{z=0} e^{\frac{ik}{2z_1}((x_1-x_0)^2+(y_1-y_0)^2)}\, dx_0\, dy_0, \tag{19}$$

which is known as the Fresnel near field diffraction integral [6].

Next, we will consider the situation of a cylindrically symmetric pinhole of radius a. First we rewrite the Fresnel near field diffraction integral in cylindrical coordinates. We start with substituting $(x_1 - x_0)^2 + (y_1 - y_0)^2$ and $dx_0\, dy_0$. We have

$$\begin{aligned}(x_1 - x_0)^2 + (y_1 - y_0)^2 &= x_1^2 + x_0^2 + y_1^2 + y_0^2 - 2x_1x_0 - 2y_1y_0 \\ &= r_1^2 + r_0^2 - 2r_1r_0\left[\cos\theta_1\cos\theta_0 + \sin\theta_1\sin\theta_0\right] \\ &= r_1^2 + r_0^2 - 2r_1r_0\cos\left(\theta_0 - \theta_1\right)\end{aligned}$$

and

$$dx_0\, dy_0 = r_0\, dr_0\, d\theta_0.$$

We substitute them into the Fresnel near field diffraction integral and set $E_{z=0} = A$, where A is a constant, which gives

$$\begin{aligned}E(P_1) &= \frac{ke^{ikz_1}}{i2\pi z_1}\int_0^a \int_{\theta_1-\frac{3\pi}{2}}^{\theta_1+\frac{\pi}{2}} Ae^{\frac{ik}{2z_1}r_1^2} e^{\frac{ik}{2z_1}r_0^2} e^{\frac{ik}{2z_1}2r_1r_0\cos(\theta_0-\theta_1)} r_0\, d\theta_0\, dr_0 \\ &= \frac{Ake^{ikz_1}}{i2\pi z_1} e^{\frac{ik}{2z_1}r_1^2}\int_0^a e^{\frac{ik}{2z_1}r_0^2} r_0 \int_{\theta_1-\frac{3\pi}{2}}^{\theta_1+\frac{\pi}{2}} e^{\frac{ik}{z_1}r_1r_0\sin(\theta_0-\theta_1+\frac{\pi}{2})}\, d\theta_0\, dr_0.\end{aligned}$$

This can be solved by letting $u = \theta_0 - \theta_1 + \frac{\pi}{2}$ and $du = d\theta_0$. This gives the solution

$$\begin{aligned}E(P_1) &= \frac{Ake^{ikz_1}}{i2\pi z_1} e^{\frac{ik}{2z_1}r_1^2}\int_0^a e^{\frac{ik}{2z_1}r_0^2} r_0 \int_{-\pi}^{\pi} e^{\frac{ik}{z_1}r_1r_0\sin(u)}\, du\, dr_0 \\ &= \frac{Ake^{ikz_1}}{iz_1} e^{\frac{ik}{2z_1}r_1^2}\int_0^a e^{\frac{ik}{2z_1}r_0^2} \mathrm{J}_0\left(\frac{kr_1r_0}{z_1}\right) r_0\, dr_0,\end{aligned} \tag{20}$$

where $\mathrm{J}_0\left(\frac{kr_1r_0}{z_1}\right)$ is a Bessel function of the first kind. Equation 20 is the solution we will use to investigate the diffraction pattern of a singular pinhole.

In order to investigate a trap's properties with m pinholes, we need to calculate the intensity at P_1 which results from the superposition of diffraction patterns of all the pinholes in our arrangement. We first need to sum together the electric fields caused by all the pinholes. This sum will look like

$$E_T = \sum_n^m E_n(P_1), \tag{21}$$

where E_n is the electric field from the nth pinhole. Next the intensity can be calculated using the formula

$$I_T = \frac{1}{2}\epsilon_o c|E_T|^2. \tag{22}$$

Using equations 20, 21, and 22 we can plot the intensity of a configuration of pinholes in order to see what a trap would look like.

2.4 Talbot Effect

The Talbot effect is a phenomenon where light illuminating a periodic structure will create exact periodic images of that structure. An example of the Talbot effect is shown in Figure 1, which was generated using a rudimentary model of a grating. It was first observed by H.F. Talbot in 1836 [7]. Talbot observed that the image of a grating would appear repeatedly after fixed distances. Following Talbot's discovery, Lord Rayleigh derived the period of this repeating image for parallel monochromatic light [8]:

$$z_T = 2\frac{l^2}{\lambda}, \tag{23}$$

where l is the period of the grating (slit distance) and λ is the wavelength of the light.

The Talbot effect may prove to be useful in exploring possible optical dipole traps. A possible configuration for a trap that takes advantage of the Talbot effect could be produced by a one-dimensional periodic mask of pinholes that a laser would shine through. Through the Talbot effect, this would create a two-dimensional array of traps because of the repetition of exact images of the pinhole mask.

While it may seem like this type of trap would work well for our application, it still requires investigation on how strong the periodic images are. If the intensity is too low, then they would not be useful in containing an atom. Because of this complication, we will also investigate traps that avoid the onset of the Talbot effect. We do this by computing intensity maps of diffraction patterns created by several different array configurations while searching for minimal Talbot effect.

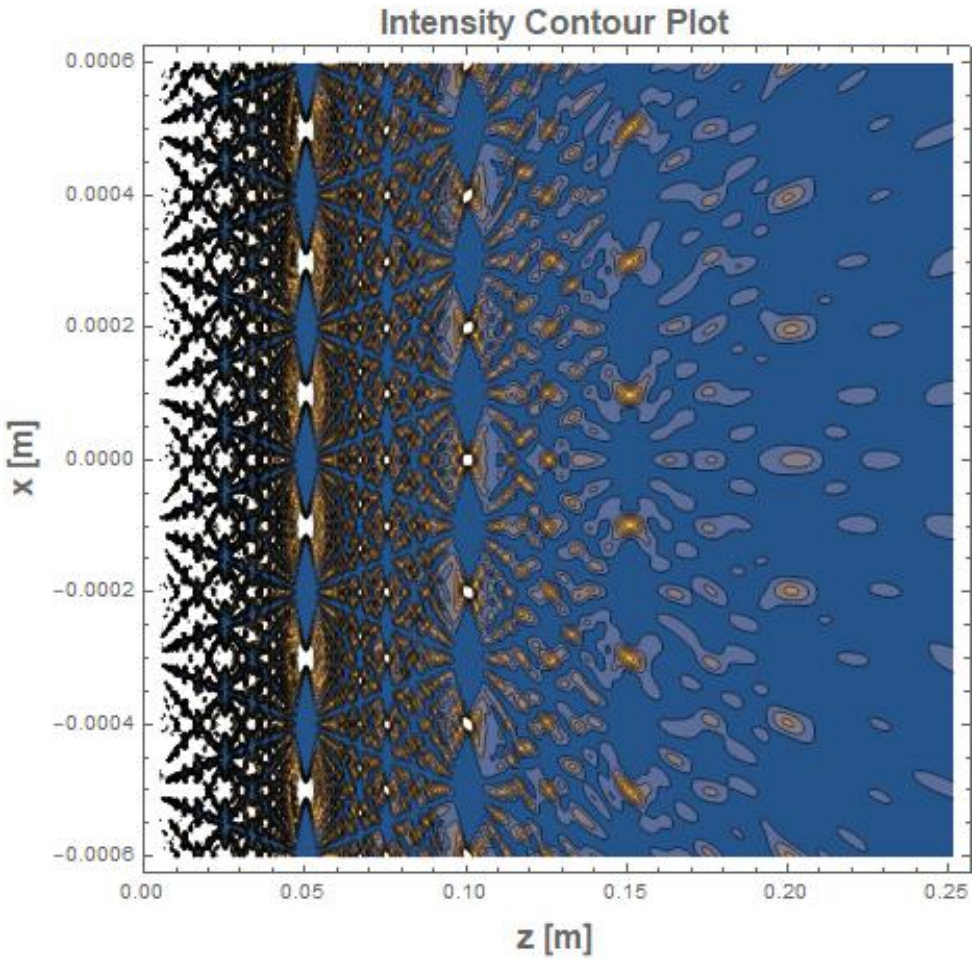

Figure 1: Talbot carpet for grating. This diagram was made using a crude model. Monochromatic light reflecting from a grating was modeled as 11 plane waves separated by 2 micrometers for each grating slit, and each slit is separated with a center to center distance of 200 micrometers. The Talbot effect can be seen at the 0.10 m mark and the 0.20 m mark.

2.5 Experimental Methods

In this section, we will discuss some ways one might load the type of traps we are discussing. The general method for loading optical dipole traps is to first cool your atoms in a vacuum chamber; second, move them to a centralized location; and finally, turn on the optical dipole traps and turn off the mechanisms used to cool and centralize the atoms. This will leave you with the optical dipole traps that are at least partially filled.

The standard way to accomplish these steps is to use a magneto-optical trap (MOT) [9]. A MOT utilizes radiative forces from laser light and a magnetic quadrupole field

created by anti-Helmholtz coils to trap atoms. Radiative forces cool atoms through a process called Doppler cooling, and the magnetic quadrupole field is able to couple with radiative forces through the Zeeman effect to centralize the atoms.

Doppler cooling works by creating a slight detuning in a laser so its frequency is slightly less than a resonance frequency in the energy structure of the atoms. When we consider the frame of reference of an atom in the vacuum chamber, we see that the frequency of light the atom experiences depends on the relative direction of motion of the light and the atom. If an atom is moving away from a light source, due to the Doppler effect the atom will experience a frequency of light that is less than the already detuned laser. This means there is a very low probability the atom will absorb any photons from this light source. However, if the atom is moving towards the light source, then due to the Doppler effect it will experience a frequency of light slightly greater than the detuned light–a frequency much closer to resonance. This means the atom will likely absorb a photon from this light source. These two amount to atoms mainly absorbing photons from light sources they are moving towards. Because of the conservation of momentum, when atoms absorb photons, they experience a momentum kick in the direction of the motion of the light, and since the atoms mainly absorb light from sources they are moving towards, they will begin to slow down or cool. In order to cool all atoms in the vacuum chamber, laser light is sent into the vacuum chamber in three perpendicular directions each with two overlapping antiparallel beams, totalling in six directed beams of light. This accounts for all possible directions of motion in the atoms.

The Zeeman effect is the splitting of spectral lines in the energy structure of an atom in the presence of a magnetic field. Near the center of a quadrupole magnetic field, the magnitude of the magnetic field exhibits an approximately linear relationship with the distance to the center. Because of this, higher amounts of splitting will be seen the further an atom is from the center. This is shown in Figure 2. Because of angular momentum selection rules, right circularly polarized light σ_+ can only produce a transition with a change in magnetic quantum number $\Delta M = +1$, while left circularly polarized light σ_- can only produce a transition with $\Delta M = -1$. This means that when atoms are to the left of the center, they will be closer to resonance with σ_+, while if they are to the right of the center, they will be more in resonance with σ_-. By directing σ_+ and σ_- laser beams appropriately, atoms will be pushed to the center of the trap.

With these two mechanisms, a MOT can effectively cool and centralize atoms in a vacuum chamber. These atoms can be directly transferred into optical dipole traps by turning on optical dipole traps in the center of the trap and turning the MOT off. Sources elaborating this process can be seen in [10], [11], and [12].

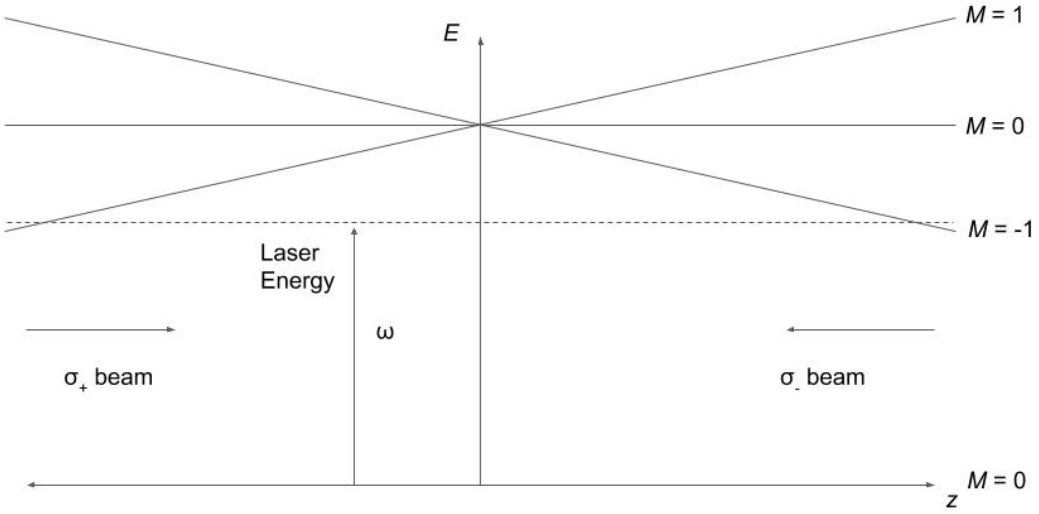

Figure 2: 1D representation of Zeeman splitting in MOT. This figure shows the gap between two states in the energy structure of an atom. The lower state is represented by the z-axis while the higher state is represented by three lines labeled $M = -1$, $M = 0$, and $M = 1$. Due to the Zeeman effect, σ_+ is closer to resonance with atoms on the left side of the center, while σ_- is closer to resonance with atoms on the right side of the center. This causes atoms to be driven towards the center [9].

3 Computational Methods

In this investigation, the equation used for the diffraction pattern of the pinholes is equation 20 discussed in Section 2.3. Since we are investigating configurations of pinholes, to calculate the total electric field at any point P_1, the superposition of all the electric fields was needed. This is shown in equation 21. Finally, to visualize the electric field, the intensity, which is shown in equation 22, was calculated in order to create a contour plot. With this contour plot, we would visually assess the usefulness of the trap. The code used for this can be seen in Appendix A.

Due to computational limits, the present calculations were restricted to one-dimensional arrays of pinholes. The fixed values that were used were the wavelength of the light λ and the magnitude of the electric field A. These values were fixed to: $\lambda = 795$ nm and $A = 100$ N/C. The variables that were explored were the pinhole radius a, the pinhole period (the distance between the center of adjacent pinholes) d, and the number of pinholes in the configuration n.

Even with limiting the arrays to one-dimensional arrays, calculating and creating a contour plot of the intensity proved to be time consuming. In order to avoid repeated lengthy computation times, methods were developed to vet which pinhole configurations would be worth investigating.

3.1 Vetting Traps

The main criteria used to vet traps was to plot the intensity of the diffraction pattern at exactly one Talbot length z_T away from the array versus position in an axis parallel to the pinhole array axis. An example of this type of graph is shown in Figure 3. Four graphs are shown with varying presence of the Talbot effect (not all configurations vetted are shown). The traps we chose to investigate further were the traps with the largest presence and the smallest presence of the Talbot effect.

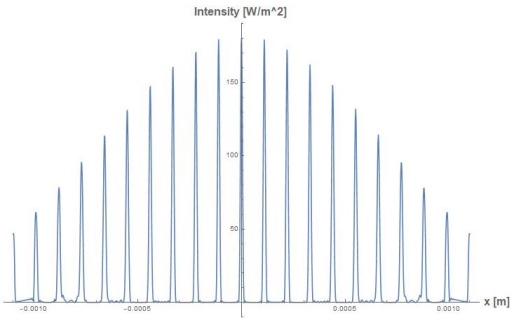

$a = 10\ \mu\text{m}$, $d = 110\ \mu\text{m}$, $n = 21$

(a)

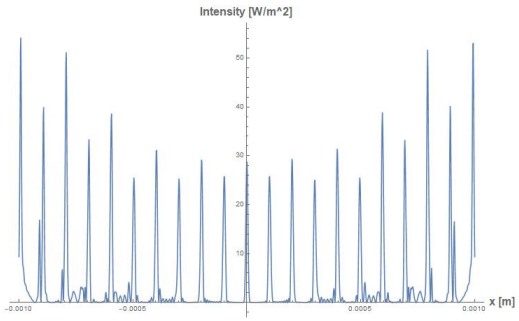

$a = 10\ \mu\text{m}$, $d = 100\ \mu\text{m}$, $n = 21$

(b)

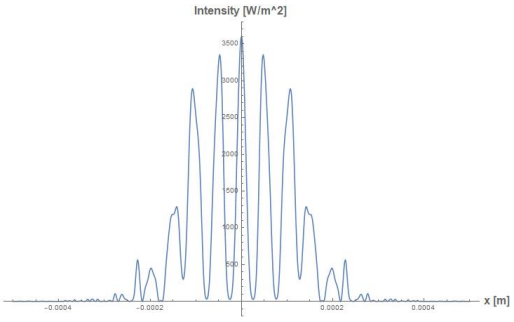

$a = 20\ \mu\text{m}$, $d = 50\ \mu\text{m}$, $n = 7$

(c)

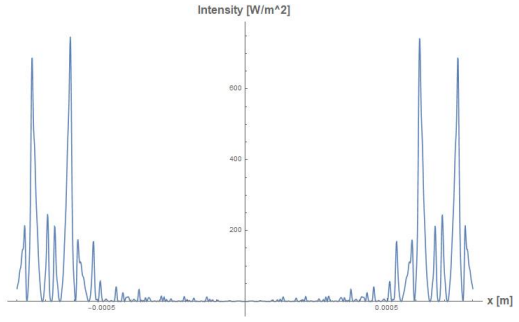

$a = 30\ \mu\text{m}$, $d = 80\ \mu\text{m}$, $n = 17$

(d)

Figure 3: Trap vetting plots. The figures are captioned with their respective values for the radius of the pinhole a, the period of the array d, and the number of pinholes in the array n. These plots illustrate a large range in the amount of presence the Talbot effect exhibits. (a) shows a large presence of the Talbot effect, (b) shows a moderate amount of presence, (c) shows a small amount of presence, and (d) shows no presence.

3.2 Trap Investigation

Traps were investigated by first making sure the intensity plots in Section 3.1 were correct. This was done by creating another intensity plot that zoomed in on two peaks. The reason for this was to make sure the resolution of our original intensity plots was not removing peaks in between the ones seen. After confirming our plot, we would then create the contour plots of the intensity as discussed in Section 3. An example of a contour plot produced can be seen in Figure 4. Once the contour plot was created, the next step would be to calculate the potential energy that the diffraction pattern and an induced dipole would create in it. The derivation for this relationship is shown in Section 2.2.

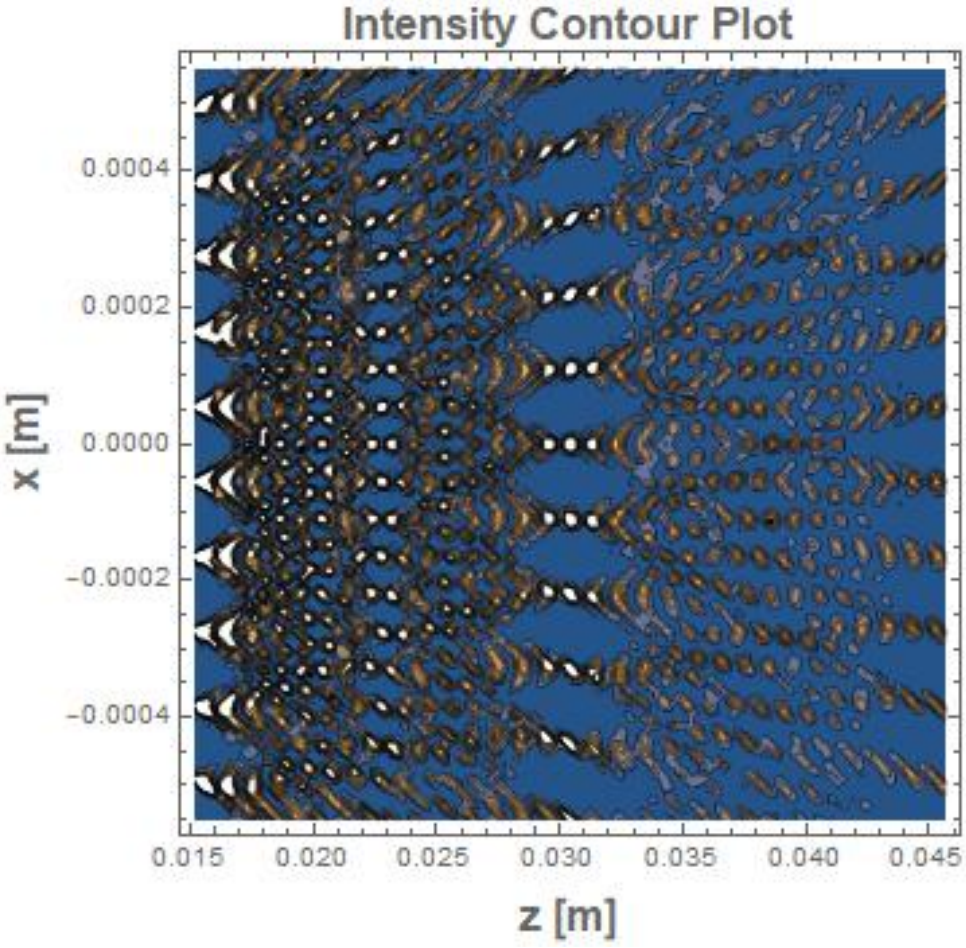

Figure 4: Talbot carpet for one-dimensional pinhole array. This contour plot was calculated with pinhole radius $a = 10$ μm, pinhole period $d = 110$ μm, and number of pinholes $n = 21$. The array of pinholes, located at the origin, is located to the left of this plot. Its replicated image can be seen in the center.

4 Results

Using the vetting methods discussed in Section 3.1, several array configurations were explored. The pinhole radius was varied between three different sizes: 10 μm, 20 μm, and 30 μm. Using the intensity plots generated at one Talbot length, the traps were visually vetted for which had the Talbot effect strongly present and weakly present. The results of this investigation can be seen in Figure 5.

These results show two promising candidates for the two different types of traps discussed. The first type of trap was the trap with weak presence of the Talbot effect. In the tables shown, a clear candidate for this type of trap was all the configurations with a pinhole period of 80 μm. Although it is not shown in the table, the onset of the Talbot effect for a period of 80 μm does not occur until 23 pinholes. The second type of trap was the trap with strong presence of the Talbot effect. Good candidates for these were the configurations with a pinhole period of 100 μm or 110 μm. The reason why these are good candidates is that their intensity plots were less noisy than the other configurations. An illustration of what this type of trap would look like can be seen in Figure 4, with the replicated image in the center serving as the atom traps.

Pinhole Radius (μm)	10								
	Pinhole Period (μm)								
Number of Pinholes	40	50	60	70	80	90	100	110	120
1	No	No	No	No	No	No	No	No	No
3	No	No	No	No	No	No	No	No	No
5	No	No	No	No	No	No	No	No	No
7	No	No	No	No	No	No	No	No	No
9	No	No	No	No	No	No	Y/N	No	Y/N
11	No	No	No	No	No	No	Yes	Yes	Yes
13	Yes	No	No	No	No	Yes	Yes	Yes	Yes
15	Yes	Yes	No	No	No	Yes	Yes	Yes	Yes
17	Yes	Yes	Yes	Yes	No	Yes	Yes	Yes	Yes
19	Yes	Yes	Yes	Yes	No	Yes	Yes	Yes	Yes
21	Yes	Yes	Yes	Yes	No	Yes	Yes	Yes	Yes

(a)

Pinhole Radius (μm)	20								
	Pinhole Period (μm)								
Number of Pinholes	40	50	60	70	80	90	100	110	120
1	NA	No	No	No	No	No	No	No	No
3	NA	No	No	No	No	No	No	No	No
5	NA	No	No	No	No	No	No	No	No
7	NA	No	No	No	No	No	No	No	No
9	NA	Y/N	No	No	No	No	No	No	No
11	NA	Yes	No	No	No	No	No	No	No
13	NA	Yes	Yes	Yes	No	No	No	No	No
15	NA	Yes	Yes	Yes	No	No	No	Y/N	No
17	NA	Yes	Yes	Yes	No	No	Y/N	Yes	Yes
19	NA	Yes	Yes	Yes	No	No	Yes	Yes	Yes
21	NA	Yes	Yes	Yes	No	Y/N	Yes	Yes	Yes

(b)

Pinhole Radius (μm)	30								
	Pinhole Period (μm)								
Number of Pinholes	40	50	60	70	80	90	100	110	120
1	NA	NA	NA	No	No	No	No	No	No
3	NA	NA	NA	No	No	No	No	No	No
5	NA	NA	NA	No	No	No	No	No	No
7	NA	NA	NA	No	No	No	No	No	No
9	NA	NA	NA	No	No	No	Y/N	No	No
11	NA	NA	NA	No	No	No	Y/N	No	Y/N
13	NA	NA	NA	Y/N	No	No	Y/N	Yes	Noisy
15	NA	NA	NA	Yes	No	Y/N	Yes	Yes	Y/N
17	NA	NA	NA	Yes	No	Y/N	Yes	Yes	Yes
19	NA	NA	NA	Yes	No	Y/N	Yes	Yes	Yes
21	NA	NA	NA	Yes	No	Yes	Yes	Yes	Yes

(c)

Figure 5: Trap vetting results. Table (a) is the result for radius $a = 10$ μm, table (b) is the result for radius $a = 20$ μm, and table (c) is the result for radius $a = 30$ μm. In the tables, "Yes" means there was substantial presence of the Talbot effect, "No" means there was not substantial presence of the Talbot effect, and "Y/N" means somewhere in between.

5 Conclusion

The traps investigated show there is promise in certain types of one-dimensional pinhole array configurations. Specifically, the configurations with pinhole period of 80 μm and 100/110 μm show promise as good candidates for pinhole diffraction traps which respectively do not and do utilize the Talbot effect. Further analysis is needed to determine the viability of these traps.

Additionally, investigation is needed for two-dimensional arrays of pinholes. If the results here, showing promise for one-dimensional arrays, extend to two-dimensional arrays, the amount of atoms these configurations could trap would scale quadratically. Investigating these may establish more possible candidates for traps of neutral atoms used for quantum computing.

6 References

[1]D. P. DiVincenzo, The physical implementation of quantum computation", Fortschritte der Physik: Progress of Physics **48**, 771–783 (2000).

[2]D. S. Weiss and M. Saffman, Quantum computing with neutral atoms", Phys. Today **70**, 44 (2017).

[3]R. Grimm, M. Weidemüller, and Y. B. Ovchinnikov, Optical dipole traps for neutral atoms", in *Advances in atomic, molecular, and optical physics*, Vol. 42 (Elsevier, 2000), pp. 95–170.

[4]R. Dumke, M. Volk, T. Müther, F. B. J. Buchkremer, G. Birkl, and W. Ertmer, Micro-optical realization of arrays of selectively addressable dipole traps: a scalable configuration for quantum computation with atomic qubits", Phys. Rev. Lett. **89**, 097903 (2002).

[5]M. Piotrowicz, M. Lichtman, K. Maller, G. Li, S. Zhang, L. Isenhower, and M. Saffman, Two-dimensional lattice of blue-detuned atom traps using a projected gaussian beam array", Physical Review A **88**, 013420 (2013).

[6]S. Guha, G. D. Gillen, and K. Gillen, *Light propagation in linear optical media* (CRC Press, 2013) Chap. 7.1.1-7.1.2.

[7]H. F. Talbot, Lxxvi. facts relating to optical science. no. iv", The London, Edinburgh, and Dublin Philosophical Magazine and Journal of Science **9**, 401–407 (1836).

[8]J. T. Winthrop and C. R. Worthington, Theory of fresnel images. i. plane periodic objects in monochromatic light", JOSA **55**, 373–381 (1965).

[9]H. J. Metcalf, P. van der Straten, and P. van der Straten, *Laser cooling and trapping (graduate texts in contemporary physics)* (Springer, 2001) Chap. 11.4.1.

[10]S. Kuppens, K. Corwin, K. Miller, T. Chupp, and C. Wieman, Loading an optical dipole trap", Physical review A **62**, 013406 (2000).

[11]K. O'Hara, S. Granade, M. Gehm, and J. Thomas, Loading dynamics of co 2 laser traps", Physical Review A **63**, 043403 (2001).

[12]D. Han, M. T. DePue, and D. S. Weiss, Loading and compressing cs atoms in a very far-off-resonant light trap", Physical Review A **63**, 023405 (2001).

7 Appendix A

Mathematica Code for Calculating Intensity

Constants:

n = 10; (*2n+1 = Number of pinholes*)
λ = 795*10^{-9}; (*Wavelength*)
k = 2*π /λ ; (*Wavenumber*)
d = 110*10^{-6}; (*Pinhole Period*)
a = 10*10^{-6}; (*Radius of Pinhole*)
A = 100; (*Magnitude of Electric Field at $z = 0$*)

Intensity:

ElectricField[z_,x_,y_,k_,a_]
$:= \mathrm{A}\frac{k\mathrm{Exp}[ikz]}{iz}\ \mathrm{Exp}\left[\frac{ik}{2z}\left(x^2+y^2\right)\right]\ \mathrm{NIntegrate}\left[\mathrm{Exp}\left[\frac{ik}{2z}r^2\right]\ \mathrm{BesselJ}\left[0, \frac{k}{z}r\sqrt{x^2+y^2}\right]\ r, \{r, 0, a\}\right]$

TotalElectric[z_,x_,y_,k_,a_,d_,n_] := $\sum_{i=-n}^{n}$ElectricField[z,x+i*d,y,k,a]

Intensity[z_,x_,y_,k_,a_,d_,n_] := Re[TotalElectric[z,x,y,k,a,d,n]]^2

Plotting:

ContourPlot[Intensity[z,x,0,k,a,d,6],{z,(d^2)/λ , 3*(d^2)/λ},{x,-5d,5d}]

Plot[Intensity[2*(d^2)/λ ,x,0,k,a,d,n],{x,-10d,10d}]